Title

Inhibiting and Remodeling Toxic Amyloid-Beta Oligomer Formation Using a Computationally Designed Drug Molecule That Targets Alzheimer's Disease

Journal

Journal of The American Society for Mass Spectrometry, 30(1)

ISSN

1044-0305

Authors

Downey, Matthew A
Giammona, Maxwell J
Lang, Christian A
et al.

Publication Date

2019

DOI

10.1007/s13361-018-1975-1

Peer reviewed

HHS Public Access

Author manuscript

J Am Soc Mass Spectrom. Author manuscript; available in PMC 2020 January 01.

Published in final edited form as:

J Am Soc Mass Spectrom. 2019 January ; 30(1): 85–93. doi:10.1007/s13361-018-1975-1.

Inhibiting and Remodeling Toxic Amyloid-beta Oligomer Formation Using a Computationally Designed Drug Molecule that Targets Alzheimer's Disease

Matthew A. Downey[1], **Maxwell J. Giammona**[1], **Christian A. Lang**[3], **Steven K. Buratto**[1], **Ambuj Singh**[2,3], and **Michael T. Bowers**[1,*]

[1]Department of Chemistry and Biochemistry, University of California, Santa Barbara, California 93106, United States

[2]Department of Computer Science, University of California, Santa Barbara, California, 93106, United States

[3]Acelot, Inc. 5385 Hollister Ave, Suite 111, Santa Barbara, CA 93111, U.S.A.

Abstract

Alzheimer's Disease (AD) is rapidly reaching epidemic status among a burgeoning aging population. Much evidence suggests the toxicity of this amyloid disease is most influenced by the formation of soluble oligomeric forms of Amyloid β-protein, particularly the 42 residue alloform (Aβ42). Developing potential therapeutics in a directed, streamlined approach to treating this disease is necessary. Here we utilize the Joint Pharmacophore Space (JPS) model to design a new molecule [AC0107] incorporating structural characteristics of known Aβ inhibitors, blood-brain barrier permeability, and limited toxicity. To test the molecule's efficacy experimentally, we employed ion mobility mass spectrometry (IM-MS) to discover [AC0107] inhibits the formation of the toxic Aβ42 dodecamer at both high (1:10) and equimolar concentrations of inhibitor. Atomic force microscopy (AFM) experiments reveal that [AC0107] prevents further aggregation of Aβ42, destabilizes preformed fibrils and reverses Aβ42 aggregation. This trend continues for long-term interaction times of 2 days until only small aggregates remain with virtually no fibrils or higher order oligomers surviving. Pairing JPS with IM-MS and AFM presents a powerful and effective first step for AD drug development.

Alzheimer's Disease (AD) is the most common neurodegenerative disorder. The economic cost of care in the United States is projected to be $1.1 trillion per year by 2050, which is nearly a 4-fold increase over estimates for 2017 [1], and this cost does not include the millions of voluntary caregivers. The cause of AD is not fully understood and there is neither a cure nor therapy to slow the progress of the disease.

AD is correlated unequivocally post-mortem by the presence of intracellular neurofibrillary tangles of hyperphosphorylated tau protein as well as extracellular amyloid plaques in the brain. These plaques are composed of proteinaceous fragments of the neuronal

*Address reprint requests to Michael T. Bowers, Department of Chemistry and Biochemistry, University of California, Santa Barbara, California 93106, USA. bowers@chem.ucsb.edu. Phone: 805-893-2893. Fax: 805-893-8703.

transmembrane Amyloid Precursor Protein (APP). There is increasing evidence that these fragments, collectively referred to as amyloid-beta (Aβ), are central to AD pathology, including inducing aberrant tau morphology [2–4]. Aβ is formed when APP is proteolytically cleaved by a series of secretases, leaving behind peptides primarily 40 and 42 residues in length, Aβ40 and Aβ42, respectively [5,6]. Both alloforms self-associate in the extracellular space and form soluble oligomers that aggregate into insoluble amyloid fibrils. Interestingly, Aβ42 is ten times less prevalent in the brain than Aβ40, but is more fibrillogenic, much more toxic, and makes up the bulk of the amyloid plaques observed with AD [7–12]. A study of transgenic 3×Tg-AD mice noted that significant extracellular accumulation of β-sheet-rich Aβ corresponded to appreciable intracellular uptake of Aβ along with cognitive deficits [12]. A neuroblastoma cell study of Aβ42 aggregation on the plasma membrane produced an analogous observation of increased cytotoxicity with internalization of Aβ42 aggregates in the intracellular domain [13]. Although large assemblies could be responsible, in part, to neurodegeneration in later stages of AD, a high plaque burden in the brain does not directly correlate to greater cognitive deficits [14–16]. Aβ fibrils may indeed be a kind of neuroprotective sink in the aggregation pathway compared to the penultimate, toxic soluble oligomers [17,18].

Fibril morphology and aggregation mechanisms are quite different for Aβ40 and Aβ42, despite both having identical sequences save for Aβ42's two additional C-terminal residues as shown in Scheme 1 below:

Aβ40 aggregation has been shown to terminate at tetramer, before going on to slowly form fibrils, but Aβ42 has growth out to dodecamer [19,20]. A 56 kilo-Dalton Aβ assembly linked to memory deficits in transgenic mice, and isolated in human cerebrospinal fluid, corresponds to the molecular weight of the Aβ42 dodecamer [9,10,17]. While the fibrils of Aβ42 are a significant neuropathological event in AD, AFM experiments showed the dodecamer of Aβ42 is vital for the initiation and seeding of fibril growth [21]. Hence, the dodecamer of Aβ42 plays a central role in AD and the inhibition of this soluble dodecamer species is key in preventing its inherent toxicity as well as subsequent pathological aspects of AD downstream.

Efforts to develop therapeutics to decrease or stop overall Aβ production by limiting secretase activity have proven unmanageable. As is typical for proteins, γ-secretase has important biological functions other than forming the C-terminus of Aβ, so altering its activity leads to reduction of neuronal calcium signaling, a decrease in lymphocyte production, and affects intestinal goblet cell differentiation [22–24]. β-secretase, which cleaves APP to form the N-terminus of Aβ, has a large catalytic pocket that would require an inhibitor too large to effectively pass the blood brain barrier [25]. Another strategy has been to up-regulate Aβ clearance mechanisms through immunotherapy, but the development of meningoencephalitis, Aβ antibody-induced cerebral hemorrhages in transgenic mice and human trials [26–28], small population datasets and very few completed Phase III drug studies for immunotherapeutics has prevented significant progress [29]. Further, removing Aβ could impair neuroprotective properties of Aβ40 and inherent amounts of Aβ in the hippocampus [30–33], suggesting that oligomeric forms of Aβ are a more amenable target for AD therapeutics.

Many compounds are known to inhibit Aβ oligomeric growth and fibril formation [34–46] but finding a potential therapeutic drug with biological efficacy is extremely challenging. Currently only a handful of drugs are FDA approved to treat AD and even fewer to treat all stages of it. One underlying factor slowing the development of therapeutics is that the detailed mechanism of AD pathology is not known. Consequently most efforts only aim to address symptoms of the disease to make it more manageable. Three immediate concerns with prospective anti-amyloid therapeutics are the compounds' ability to pass the blood-brain barrier, toxicity to other bodily systems, and Aβ42 specificity. It is therefore of keen interest to find a directed approach for screening potential inhibitors of pre-fibril amyloid aggregation that also incorporate these concerns before the long and expensive process of drug trials are initiated.

Utilization of the Joint Pharmacophore Space (JPS) model [47,48] to find potential therapeutics provides an *in silico*, first step in the drug discovery process. By accessing data on millions of compounds from cell-based assays, a database can be constructed for any attribute of a compound and then overlap those results with any number of other qualities from other assays. A machine learning algorithm then constructs a list of compounds ranked by probabilistic methods for the most positive hits for all the qualities desired. Because the detailed mechanism of AD is not understood, it is important to emphasize that this approach does not single out one particular biological target. It takes into account a compound's overall geometry of functional groups relative to other structural characteristics that have satisfied blood-brain permeability, low toxicity, and interaction with Aβ42 with no specific target in mind. Using these criteria, JPS can design new compounds that are more likely to have a directed impact on pathological aspects of AD.

To test this process experimentally, we have employed ion mobility mass spectrometry (IM-MS) and atomic force microscopy (AFM) to study the effect one high-scoring JPS generated compound [AC0107] (Scheme 2) has on Aβ42 assembly as well as its ability to remodel pre-formed Aβ42 fibrils.

METHODS

Ion Mobility Mass Spectrometry Experiments

Aβ42 wild type peptides were synthesized by FMOC chemistry, purified by reverse-phase HPLC, verified through mass spectrometry and amino acid analysis as previously described [49] and lyophilized. Bulk peptides were subsequently dissolved in hexafluoroisopropanol (Sigma-Aldrich, St. Louis), aliquoted to individual vials, lyophilized again and stored at −20°C. Prior to ion mobility experiments, peptides were solvated with 10mM ammonium acetate buffer (pH 7.4) to a final peptide concentration of 10 μM. To prevent rapid aggregation and to increase ion signal, samples were kept on ice for the duration of the study. To study the effect of the inhibitor on Aβ42 assembly, mass spectra and arrival time distributions (ATDs) were collected first of Aβ42 alone and then inhibitor ([AC0107] provided by Acelot, Inc.) was added to the same solution to form a 1:10 peptide:inhibitor concentration ratio and the data was collected again. The same recovery experiment was carried out for a 1:1 concentration ratio as well. Incubation times indicate the time after solvation of Aβ42 at which signal was acquired during repeat experiments.

All ion mobility and mass spectrometry experiments were performed on a home-built electrospray ionization ion mobility mass spectrometer [50]. To acquire a mass spectrum, ions are generated via an applied potential difference between a gold-coated nanoelectrospray glass capillary tip and the capillary inlet of the mass spectrometer. The ions then travel through an ion funnel and are then injected into a 4.503 cm drift cell filled with ~3.5 torr helium. Upon leaving the drift cell, ions are mass analyzed by a quadrupole mass filter and detected by a conversion dynode and channel electron multiplier.

For mobility experiments, ions are stored in the ion funnel and then pulsed at regular intervals into the drift cell at low energy. Once inside, ions travel through a helium buffer gas under the influence of a weak, homogeneous electric field, E The ions quickly come to thermal equilibrium and reach a constant drift velocity, v_d. Higher order oligomers have more charge and more compact component monomer cross-sections than those of a lower order and travel more quickly through the drift cell at constant pressure. The mobility is obtained from Eqn 1:

$$K = \frac{v_d}{E} \quad (1)$$

The ion mobility is dependent on both pressure and temperature and is converted to its reduced form:

$$K_0 = K\frac{P}{760}\frac{273.15}{T} \quad (2)$$

with pressure P in torr and temperature T in Kelvin.

The reduced mobility is determined by plotting the arrival time versus P/V ratio where V is the voltage across the cell. The arrival time t_a is given in Eqn 3:

$$t_a = \frac{L}{v_d} = \frac{L}{KE} = \frac{L^2(273.15)}{K_0(760)T}\frac{P}{V} - t_0 \quad (3)$$

where L is the drift cell length, t_0 the time the ions spend outside the drift cell before reaching the detector.

After leaving the drift cell, ions are mass-selected, and detected as a function of the arrival time to produce an arrival time distribution (ATD). An ion's mobility is related to its collision cross-section σ as shown in Eqn 4 [51]:

$$\sigma = \frac{3}{16}\left(\frac{2\pi}{\mu kT}\right)^{\frac{1}{2}}\frac{e}{N_0 K_0} \quad (4)$$

where μ is the reduced mass of the ion and helium buffer gas, k the Boltzmann constant, e the charge of the ion, and N_0 the buffer gas density.

AFM Experiments

Samples were prepared for AFM experiments by depositing 50 μL of 10 μM Aβ42 prepared in a 10 mM ammonium acetate buffer with the stated concentration of inhibitor onto freshly cleaved V1-grade mica (TedPella, Redding, CA) and dried in a desiccator. Tapping-mode AFM images were acquired from the dried samples in air using an MFP-3D Atomic Force Microscope (Asylum Research, Goleta, CA). High resolution silicon probe tips with a tip radius of 1 nm, a cantilever spring constant of 7 N/m and a resonant frequency of 155 kHz (MikroMasch USA, Lady's Island, SC) were used to acquire the AFM images. All AFM images were collected in the repulsive force regime.

JPS In Silico Model

To train the JPS, a collection of 30 known Aβ inhibitors [35–46] were used to better recognize chemical topologies necessary for Aβ inhibition. With the JPS trained, the ZINC collection [52] was screened for compounds that incorporated structures more likely to inhibit Aβ self-assembly that also exhibited blood-brain barrier (BBB) permeability and minimal toxicity. A shortlist of compounds was populated and then subjected to Caco-2 and hERG assays to give preliminary BBB permeability and toxicity information. The remaining compounds were subjected to a sensitive trafficking assay [53,54] to test their ability to inhibit membrane trafficking of Aβ. [AC0107] is the first of the JPS-generated compounds to be tested experimentally.

RESULTS and DISCUSSION

IM-MS Experiments

Three peaks are present in the mass spectrum for Aβ42 wt alone: an electrospray-induced, monomer charge state z/n= −4, a monomer solution state z/n= −3, and an oligomer peak at z/n= −5/2 (Fig. 1a). (All monomer z/n data is provided in the Supporting Information). Upon addition of the inhibitor, the same charge states are observed, with no complex peak formation for either 1:10 or 1:1 concentrations (Fig. 1b,c). Even though there is no apparent binding of the inhibitor to Aβ42 in the mass spectrum, the ATD of the −5/2 peak is very different (Fig. 1d–h). Prior to addition of inhibitor we observe the same oligomeric structures previously assigned as dimer, tetramer, hexamer, decamer, and dodecamer (n= 2, 4, 6, 10, and 12, respectively) [19,20]. After 1 hour co-incubation with 1:10 inhibitor, the decamer and dodecamer ATD features are essentially eliminated.

At 1 hour the hexamer peak is also significantly diminished with the tetramer and dimer feature unchanged. At 24 hours 1:10 co-incubation the dodecamer disappears completely with oligomerization up to hexamer still present.

The same set of experiments were performed at a lower 1:1 Aβ42:[AC0107] ratio (Fig. 1c, 1f, 1h). After 1 hour co-incubation under these conditions, all oligomers of order n > 6 are completely inhibited. At 24 hours 1:1 co-incubation, there is an increase in hexamer and

decrease in dimer relative to the tetramer feature; but the dodecamer peak is still absent indicating [AC0107] prevents the dodecamer from forming.

We observe similar Aβ42 wt monomer cross sections as previously published [19,55,56] both with and without the inhibitor (Table 1). This indicates that introduction of [AC0107] does not affect Aβ42 native monomer structure in our experiments (Fig. S1,S2). Interestingly, binding of the inhibitor to Aβ42 of any charge state is not observed. It is possible that the binding of the compound to full-length Aβ42 is not sustained under the conditions of the electrospray process, but clearly the disruption of cytotoxic oligomers of Aβ42 in solution is occurring.

AFM Experiments

Atomic Force Microscopy (AFM) was utilized to study the effect of the inhibitor on the formation of larger scale aggregates and to determine the effect it may have on pre-formed aggregates and fibrils. A 50 μL aliquot of 10 μM Aβ42 solution in 10 mM ammonium acetate was removed and drop-cast onto a mica disc, dried at ambient conditions in a desiccator and imaged. It takes approximately 5 minutes to prepare the peptide and for the disc to dry, making it the earliest time Aβ42 aggregation can be observed. After 5 minutes incubation, large globular aggregates have formed but few fibrils are observed (Fig. 2a). By 30 minutes, fibril features emerge along with higher order oligomers (heights of 2–6 nm) (Fig. 2b). After 60 minutes, the trend toward higher fibril content and larger oligomers continues (Fig. 2c). The rapid formation of plentiful fibrils and globular aggregates is consistent with AFM studies at high concentration [57]. Particle height distributions (Fig. S3) show quantitatively what is shown visually in the AFM topography images. Over time, the ratio of higher order oligomers to lower order oligomers (particle heights less than 1 nm) increases with an overall decrease in the number of particles present. This can be attributed to smaller oligomers converting into larger ones and larger oligomers going on to form fibrils.

Data for a 10-fold excess of inhibitor added to the same solution of pre-incubated Aβ42 are shown in Fig. 2d, e, and f. After 5 minutes with [AC0107], the AFM image (Fig. 2d) is morphologically similar to Aβ42 alone at 60 min, but by 30 minutes co-incubation there is a massive shift toward small oligomeric structures relative to large aggregates (Fig. 2e) and after 60 minutes a peptide film is observed on the mica disc and few fibrils and distinct oligomeric features persist (Fig. 2f).

The same AFM experiment was repeated at a lower 1:1 Aβ42:[AC0107] concentration ratio. After 5 minutes of co-incubation with the inhibitor, the pre-formed fibrils are still well-established but by 30 minutes fibrils are diminished, indicating that [AC0107] is still effective at interrupting Aβ42 self-assembly at low concentrations (Fig. 2h). The particle height distribution for the 30-minute image results in a surprising decrease in low order oligomers (heights less than 1 nm) relative to higher order ones. What is likely happening is the disaggregating effect of [AC0107] continues but lower order oligomers self-associate into a film with higher order structures depositing on top of them, showing an apparent decrease in lower order oligomers. These trends are sustained for the 60-minute image (Fig. 2i) with the continued breakup of pre-formed fibrils and the decrease in apparent number of

lower order oligomers, both in support of [AC0107] as an effective inhibitor of Aβ aggregation.

Interpretation of AFM phase imaging sheds light on compositional characteristics of deposited material on the mica surface. Phase shifts of the oscillating cantilever as the AFM probe scans the features on the mica surface provides information about the energy dissipation when the probe tip interacts with the sample. When the probe interacts with particles that are hard (i.e. more structured), less energy is dissipated resulting in a phase shift toward 90° relative to the background media of the image. When the probe interacts with particles that are soft (less structured), more energy is dissipated and the phase shifts away from 90° relative to the background media of the image. We will use this rationale as a measure of the internal order of the amyloid fibrils on the mica surface. Variance in phase signal is commonplace among different samples and probes, but the observed phase shift relative to structures within the image are consistent [58–60]. Figure 3a–c shows phase images of Aβ42 incubated in solution for 5, 30, and 60 minutes, respectively. As expected, the axes of the fibrils smoothen and are hard (i.e. ordered) relative to the background indicating fibril stability increases over time. Fewer distinct oligomeric assemblies are present as fibrils grow and lengthen (Fig. 3c). Upon introduction of 1:1 inhibitor to the same solution, the fibril axis adopts a beads-on-a-string appearance, softens relative to the ordered fibrils, distinct oligomeric features become more represented, and the negative phase shift relative to the background has disappeared after the 60 minutes co-incubation (Fig. 3d–f), similar to the peptide film observed at 1:10 [AC0107] at the same time point (Fig. 2f). Through our IM-MS experiments we verified that higher order oligomer (Aβ42 dodecamer) formation is being disrupted in the presence of [AC0107] (Fig. 1). Here we observe a phase shift from harder to softer structures, and given that there is no reason to believe that monomers and lower order oligomers would normally get softer over time, it is reasonable that the internal order of the fibrils is becoming less structured due to the presence of [AC0107]. These data indicate [AC0107] destabilizes and reverses normal Aβ42 fibril assembly and encourages Aβ42 to behave more like the less cytotoxic Aβ40.

To assess the steady state of Aβ42 aggregation in the presence of the [AC0107], the two were pre-mixed and incubated for 24 and 48 hours and analyzed by AFM. At 24 hours there is little to no discrete oligomeric structures present (Fig. 4a) though there are fully developed fibrils with 7nm diameters, either alone or bundled together. This indicates that fibril formation is possible even in the presence of [AC0107] but it must occur by another pathway outside the dodecamer seeding mechanism [21] because dodecamer formation is completely inhibited shortly after addition of [AC0107] to Aβ42 solution as seen in our IM-MS experiments. Zooming in on both backgrounds of the 1:10 and 1:1 24hr images (Fig. 4b and e, respectively) we can see a somewhat filamentous network of 1 nm tall structures, strikingly similar to what was observed with Aβ40 incubated at 30+ minutes [21]. At 48 hours incubation with [AC0107], the fibril content is essentially zero for both 1:10 and 1:1 concentration ratios (Fig. 4c and f, respectively). Interestingly, even the peptide film observed at earlier time points has broken up into discrete aggregates.

CONCLUSIONS

Aβ42 adopts a planar hexamer ring structure that stacks on another hexamer to form the toxic, stacked dodecamer species [19]. Amyloid inhibitors are thought to interrupt π-π stacking of aromatic chains that contribute to β-sheet structure as aggregation progresses [61,62,63]. It is possible [AC0107] acts this way as well. However because no complexes of Aβ42 and [AC0107] are observed in our study, the details of the molecular interaction between Aβ42 and [AC0107] remain unclear.

Our data indicate [AC0107] initiates a reversal of the aggregation pathway of Aβ42 over the timescale of our experiments, interrupting the formation of Aβ42 higher order oligomers. AFM experiments show Aβ42 assembly in mixtures with [AC0107] behaves like the neuroprotective alloform Aβ40. This work supports the fact that if Aβ42 dodecamers are critical to the rapid fibrillization of Aβ42. These results indicate the small molecules designed by JPS are effective and sets the stage for a more cost-effective and direct screening strategy to combat AD.

Supplementary Material

Refer to Web version on PubMed Central for supplementary material.

Acknowledgments

The authors gratefully acknowledge support from the National Institute of Health – National Institute of Aging under grant 1R01AG047116 (M.T.B.) and funding through MURI and DURIP programs of the U.S. Army Research Office under Grant Nos. DAAD 19-03-1-0121 and W911NF-09-1-0280 for the purchase of the AFM instrument (S.K.B.).

References

1. 2017 Alzheimer’s disease facts and figures. Alzheimer’s & Dementia: The Journal of the Alzheimer’s Association 13 (4), 325–373.
2. Götz J; Chen F; van Dorpe J; Nitsch RM, Formation of Neurofibrillary Tangles in P301L Tau Transgenic Mice Induced by Aβ42 Fibrils. Science (New York, N.Y.) 2001, 293 (5534), 1491.
3. Lewis J; Dickson DW; Lin W-L; Chisholm L; Corral A; Jones G; Yen S-H; Sahara N; Skipper L; Yager D; Eckman C; Hardy J; Hutton M; McGowan E, Enhanced Neurofibrillary Degeneration in Transgenic Mice Expressing Mutant Tau and APP. Science (New York, N.Y.) 2001, 293 (5534), 1487.
4. Umeda T; Maekawa S; Kimura T; Takashima A; Tomiyama T; Mori H, Neurofibrillary tangle formation by introducing wild-type human tau into APP transgenic mice. Acta neuropathologica 2014, 127 (5), 685–698. [PubMed: 24531886]
5. Haass C; Schlossmacher MG; Hung AY; Vigo-Pelfrey C; Mellon A; Ostaszewski BL; Lieberburg I; Koo EH; Schenk D; Teplow DB; Selkoe DJ, Amyloid β-peptide is produced by cultured cells during normal metabolism. Nature 1992, 359, 322. [PubMed: 1383826]
6. Takami M; Nagashima Y; Sano Y; Ishihara S; Morishima-Kawashima M; Funamoto S; Ihara Y, γ-Secretase: Successive Tripeptide and Tetrapeptide Release from the Transmembrane Domain of β-Carboxyl Terminal Fragment. The Journal of Neuroscience 2009, 29 (41), 13042. [PubMed: 19828817]
7. Jakob-Roetne R; Jacobsen H, Alzheimer’s Disease: From Pathology to Therapeutic Approaches. Angewandte Chemie International Edition 2009, 48 (17), 3030–59. [PubMed: 19330877]

8. Dahlgren KN; Manelli AM; Stine WB; Baker LK; Krafft GA; LaDu MJ, Oligomeric and Fibrillar Species of Amyloid-β Peptides Differentially Affect Neuronal Viability. Journal of Biological Chemistry 2002, 277 (35), 32046–32053. [PubMed: 12058030]

9. Lesné S; Koh MT; Kotilinek L; Kayed R; Glabe CG; Yang A; Gallagher M; Ashe KH, A specific amyloid-β protein assembly in the brain impairs memory. Nature 2006, 440, 352. [PubMed: 16541076]

10. Cheng IH; Scearce-Levie K; Legleiter J; Palop JJ; Gerstein H; Bien-Ly N; Puoliväli J; Lesné S; Ashe KH; Muchowski PJ; Mucke L, Accelerating Amyloid-β Fibrillization Reduces Oligomer Levels and Functional Deficits in Alzheimer Disease Mouse Models. Journal of Biological Chemistry 2007, 282 (33), 23818–23828. [PubMed: 17548355]

11. Mann DM; Iwatsubo T; Ihara Y; Cairns NJ; Lantos PL; Bogdanovic N; Lannfelt L; Winblad B; Maat-Schieman ML; Rossor MN, Predominant Deposition of Amyloid-β42(43) in Plaques in Cases of Alzheimer's Disease and Hereditary Cerebral Hemorrhage Associated with Mutations in the Amyloid Precursor Protein Gene. The American Journal of Pathology 1996, 148 (4), 1257–1266. [PubMed: 8644866]

12. Billings LM; Oddo S; Green KN; McGaugh JL; LaFerla FM, Intraneuronal Aβ Causes the Onset of Early Alzheimer's Disease-Related Cognitive Deficits in Transgenic Mice. Neuron 2005, 45 (5), 675–688. [PubMed: 15748844]

13. Jin S; Kedia N; Illes-Toth E; Haralampiev I; Prisner S; Herrmann A; Wanker EE; Bieschke J, Amyloid-β(1–42) Aggregation Initiates Its Cellular Uptake and Cytotoxicity. Journal of Biological Chemistry 2016, 291 (37), 19590–19606. [PubMed: 27458018]

14. Dodart J-C; Bales KR; Gannon KS; Greene SJ; DeMattos RB; Mathis C; DeLong CA; Wu S; Wu X; Holtzman DM; Paul SM, Immunization reverses memory deficits without reducing brain Aβ burden in Alzheimer's disease model. Nature Neuroscience 2002, 5, 452. [PubMed: 11941374]

15. Gandy S; Simon AJ; Steele JW; Lublin AL; Lah JJ; Walker LC; Levey AI; Krafft GA; Levy E; Checler F; Glabe C; Bilker WB; Abel T; Schmeidler J; Ehrlich ME, Days to criterion as an indicator of toxicity associated with human Alzheimer amyloid-β oligomers. Annals of Neurology 2010, 68 (2), 220–230. [PubMed: 20641005]

16. Erten-Lyons D; Woltjer RL; Dodge H; Nixon R; Vorobik R; Calvert JF; Leahy M; Montine T; Kaye J, Factors associated with resistance to dementia despite high Alzheimer disease pathology. Neurology 2009, 72 (4), 354. [PubMed: 19171833]

17. Lesné SE; Sherman MA; Grant M; Kuskowski M; Schneider JA; Bennett DA; Ashe KH, Brain amyloid-β oligomers in aging and Alzheimer's disease. Brain 2013, 136 (5), 1383–1398. [PubMed: 23576130]

18. Sakono M; Zako T, Amyloid oligomers: formation and toxicity of Aβ oligomers. FEBS Journal 2010, 277 (6), 1348–1358. [PubMed: 20148964]

19. Bernstein SL; Dupuis NF; Lazo ND; Wyttenbach T; Condron MM; Bitan G; Teplow DB; Shea J-E; Ruotolo BT; Robinson CV; Bowers MT, Amyloid-β protein oligomerization and the importance of tetramers and dodecamers in the aetiology of Alzheimer's disease. Nature chemistry 2009, 1, 326.

20. Bernstein SL; Wyttenbach T; Baumketner A; Shea J-E; Bitan G; Teplow DB; Bowers MT, Amyloid β-Protein: Monomer Structure and Early Aggregation States of Aβ42 and Its Pro19 Alloform. Journal of the American Chemical Society 2005, 127 (7), 2075–2084. [PubMed: 15713083]

21. Economou NJ; Giammona MJ; Do TD; Zheng X; Teplow DB; Buratto SK; Bowers MT, Amyloid β-Protein Assembly and Alzheimer's Disease: Dodecamers of Aβ42, but Not of Aβ40, Seed Fibril Formation. Journal of the American Chemical Society 2016, 138 (6), 1772–1775. [PubMed: 26839237]

22. Leissring MA; Murphy MP; Mead TR; Akbari Y; Sugarman MC; Jannatipour M; Anliker B; Müller U; Saftig P; De Strooper B; Wolfe MS; Golde TE; LaFerla FM, A physiologic signaling role for the γ-secretase-derived intracellular fragment of APP. Proceedings of the National Academy of Sciences 2002, 99 (7), 4697.

23. Wong GT; Manfra D; Poulet FM; Zhang Q; Josien H; Bara T; Engstrom L; Pinzon-Ortiz M; Fine JS; Lee H-JJ; Zhang L; Higgins GA; Parker EM, Chronic Treatment with the γ-Secretase Inhibitor LY-411,575 Inhibits β-Amyloid Peptide Production and Alters Lymphopoiesis and Intestinal Cell

Differentiation. Journal of Biological Chemistry 2004, 279 (13), 12876–12882. [PubMed: 14709552]

24. Milano J; McKay J; Dagenais C; Foster-Brown L; Pognan F; Gadient R; Jacobs RT; Zacco A; Greenberg B; Ciaccio PJ, Modulation of Notch Processing by γ-Secretase Inhibitors Causes Intestinal Goblet Cell Metaplasia and Induction of Genes Known to Specify Gut Secretory Lineage Differentiation. Toxicological Sciences 2004, 82 (1), 341–358. [PubMed: 15319485]
25. Ghosh AK; Osswald HL, BACE1 (β-secretase) inhibitors for the treatment of Alzheimer's disease. Chemical Society Reviews 2014, 43 (19), 6765–6813. [PubMed: 24691405]
26. Wilcock DM; Rojiani A; Rosenthal A; Subbarao S; Freeman MJ; Gordon MN; Morgan D, Passive immunotherapy against Aβ in aged APP-transgenic mice reverses cognitive deficits and depletes parenchymal amyloid deposits in spite of increased vascular amyloid and microhemorrhage. Journal of Neuroinflammation 2004, 1, 24–24. [PubMed: 15588287]
27. Pfeifer M; Boncristiano S; Bondolfi L; Stalder A; Deller T; Staufenbiel M; Mathews PM; Jucker M, Cerebral Hemorrhage After Passive Anti-Aβ Immunotherapy. Science (New York, N.Y.) 2002, 298 (5597), 1379.
28. Ferrer I; Rovira MB; Guerra MLS; Rey MJ; Costa-Jussá F, Neuropathology and Pathogenesis of Encephalitis following Amyloid β Immunization in Alzheimer's Disease. Brain Pathology 2004, 14, 11–20. [PubMed: 14997933]
29. Gilman S; Koller M; Black RS; Jenkins L; Griffith SG; Fox NC; Eisner L; Kirby L; Rovira MB; Forette F; Orgogozo JM, Clinical effects of Aβ immunization (AN1792) in patients with AD in an interrupted trial. Neurology 2005, 64 (9), 1553. [PubMed: 15883316]
30. Puzzo D; Privitera L; Leznik E; Fà M; Staniszewski A; Palmeri A; Arancio O, Picomolar Amyloid-β Positively Modulates Synaptic Plasticity and Memory in Hippocampus. The Journal of Neuroscience 2008, 28 (53), 14537. [PubMed: 19118188]
31. Giuffrida ML; Caraci F; Pignataro B; Cataldo S; De Bona P; Bruno V; Molinaro G; Pappalardo G; Messina A; Palmigiano A; Garozzo D; Nicoletti F; Rizzarelli E; Copani A, β-Amyloid Monomers Are Neuroprotective. The Journal of Neuroscience 2009, 29 (34), 10582. [PubMed: 19710311]
32. Zou K; Gong J-S; Yanagisawa K; Michikawa M, A Novel Function of Monomeric Amyloid β-Protein Serving as an Antioxidant Molecule against Metal-Induced Oxidative Damage. The Journal of Neuroscience 2002, 22 (12), 4833. [PubMed: 12077180]
33. Kim J; Onstead L; Randle S; Price R; Smithson L; Zwizinski C; Dickson DW; Golde T; McGowan E, Aβ40 Inhibits Amyloid Deposition in Vivo. The Journal of Neuroscience 2007, 27 (3), 627–33. [PubMed: 17234594]
34. Härd T; Lendel C, Inhibition of Amyloid Formation. Journal of Molecular Biology 2012, 421 (4), 441–465. [PubMed: 22244855]
35. Scherzer-Attali R; Farfara D; Cooper I; Levin A; Ben-Romano T; Trudler D; Vientrov M; Shaltiel-Karyo R; Shalev DE; Segev-Amzaleg N; Gazit E; Segal D; Frenkel D, Naphthoquinone-tyrptophan reduces neurotoxic Aβ*56 levels and improves cognition in Alzheimer's disease animal model. Neurobiology of Disease 2012, 46 (3), 663–672. [PubMed: 22449754]
36. Ryan TM; Roberts BR; McColl G; Hare DJ; Doble PA; Li Q-X; Lind M; Roberts AM; Mertens HDT; Kirby N; Pham CLL; Hinds MG; Adlard PA; Barnham KJ; Curtain CC; Masters CL, Stabilization of Nontoxic Aβ-Oligomers: Insights into the Mechanism of Action of Hydroxyquinolines in Alzheimer's Disease. The Journal of Neuroscience 2015, 35 (7), 2871. [PubMed: 25698727]
37. Zheng X; Liu D; Klärner F-G; Schrader T; Bitan G; Bowers MT, Amyloid β-Protein Assembly: The Effect of Molecular Tweezers CLR01 and CLR03. The Journal of Physical Chemistry B 2015, 119 (14), 4831–4841. [PubMed: 25751170]
38. Lee S; Zheng X; Krishnamoorthy J; Savelieff MG; Park HM; Brender JR; Kim JH; Derrick JS; Kochi A; Lee HJ; Kim C; Ramamoorthy A; Bowers MT; Lim MH, Rational Design of a Structural Framework with Potential Use to Develop Chemical Reagents That Target and Modulate Multiple Facets of Alzheimer's Disease. Journal of the American Chemical Society 2014, 136 (1), 299–310. [PubMed: 24397771]
39. Zheng X; Gessel MM; Wisniewski ML; Viswanathan K; Wright DL; Bahr BA; Bowers MT, Z-Phe-Ala-diazomethylketone (PADK) Disrupts and Remodels Early Oligomer States of the

Alzheimer Disease Aβ42 Protein. Journal of Biological Chemistry 2012, 287 (9), 6084–6088. [PubMed: 22253440]

40. LeVine H; Ding Q; Walker JA; Voss RS; Augelli-Szafran CE, Clioquinol and other hydroxyquinoline derivatives inhibit Aβ(1–42) oligomer assembly. Neuroscience Letters 2009, 465 (1), 99–103. [PubMed: 19664688]
41. Rammes G; Gravius A; Ruitenberg M; Wegener N; Chambon C; Sroka-Saidi K; Jeggo R; Staniaszek L; Spanswick D; O'Hare E; Palmer P; Kim E-M; Bywalez W; Egger V; Parsons CG, MRZ-99030 – A novel modulator of Aβ aggregation: II – Reversal of Aβ oligomer-induced deficits in long-term potentiation (LTP) and cognitive performance in rats and mice. Neuropharmacology 2015, 92, 170–182. [PubMed: 25637092]
42. Arai T; Sasaki D; Araya T; Sato T; Sohma Y; Kanai M, A Cyclic KLVFF-Derived Peptide Aggregation Inhibitor Induces the Formation of Less-Toxic Off-Pathway Amyloid-β Oligomers. ChemBioChem 2014, 15 (17), 2577–2583. [PubMed: 25262917]
43. Hayden EY; Yamin G; Beroukhim S; Chen B; Kibalchenko M; Jiang L; Ho L; Wang J; Pasinetti GM; Teplow DB, Inhibiting amyloid β-protein assembly: Size–activity relationships among grape seed-derived polyphenols. Journal of Neurochemistry 2015, 135 (2), 416–430. [PubMed: 26228682]
44. Taylor M; Moore S; Mayes J; Parkin E; Beeg M; Canovi M; Gobbi M; Mann DMA; Allsop D, Development of a Proteolytically Stable Retro-Inverso Peptide Inhibitor of β-Amyloid Oligomerization as a Potential Novel Treatment for Alzheimer's Disease. Biochemistry 2010, 49 (15), 3261–3272. [PubMed: 20230062]
45. Yamin G; Ruchala P; Teplow DB, A Peptide Hairpin Inhibitor of Amyloid β-Protein Oligomerization and Fibrillogenesis. Biochemistry 2009, 48 (48), 11329–11331. [PubMed: 19877710]
46. Yang F; Lim GP; Begum AN; Ubeda OJ; Simmons MR; Ambegaokar SS; Chen PP; Kayed R; Glabe CG; Frautschy SA; Cole GM, Curcumin Inhibits Formation of Amyloid β Oligomers and Fibrils, Binds Plaques, and Reduces Amyloid in Vivo. Journal of Biological Chemistry 2005, 280 (7), 5892–5901. [PubMed: 15590663]
47. Ranu S; Singh AK, Novel Method for Pharmacophore Analysis by Examining the Joint Pharmacophore Space. Journal of Chemical Information and Modeling 2011, 51 (5), 1106–1121. [PubMed: 21488651]
48. Lang CA; Ray SS; Liu M; Singh AK; Cuny GD, Discovery of LRRK2 inhibitors using sequential in silico joint pharmacophore space (JPS) and ensemble docking. Bioorganic & Medicinal Chemistry Letters 2015, 25 (13), 2713–2719. [PubMed: 25998502]
49. Lomakin A; Chung DS; Benedek GB; Kirschner DA; Teplow DB, On the nucleation and growth of amyloid beta-protein fibrils: Detection of nuclei and quantitation of rate constants. Proceedings of the National Academy of Sciences of the United States of America 1996, 93 (3), 1125–1129. [PubMed: 8577726]
50. Wyttenbach T; Kemper PR; Bowers MT, Design of a new electrospray ion mobility mass spectrometer. International Journal of Mass Spectrometry 2001, 212 (1), 13–23.
51. Mason EA & McDaniel EW: Transport Properties of Ions in Gases. Wiley, New York (1988)
52. Irwin JJ; Shoichet BK, ZINC − A Free Database of Commercially Available Compounds for Virtual Screening. Journal of Chemical Information and Modeling 2005, 45 (1), 177–182. [PubMed: 15667143]
53. Izzo NJ; Staniszewski A; To L; Fa M; Teich AF; Saeed F; Wostein H; Walko T, 3rd; Vaswani A; Wardius M; Syed Z; Ravenscroft J; Mozzoni K; Silky C; Rehak C; Yurko R; Finn P; Look G; Rishton G; Safferstein H; Miller M; Johanson C; Stopa E; Windisch M; Hutter-Paier B; Shamloo M; Arancio O; LeVine H, 3rd; Catalano SM, Alzheimer's therapeutics targeting amyloid beta 1–42 oligomers I: Abeta 42 oligomer binding to specific neuronal receptors is displaced by drug candidates that improve cognitive deficits. PloS one 2014, 9 (11), e111898. [PubMed: 25390368]
54. Izzo NJ; Xu J; Zeng C; Kirk MJ; Mozzoni K; Silky C; Rehak C; Yurko R; Look G; Rishton G; Safferstein H; Cruchaga C; Goate A; Cahill MA; Arancio O; Mach RH; Craven R; Head E; LeVine H, 3rd; Spires-Jones TL; Catalano SM, Alzheimer's therapeutics targeting amyloid beta 1–42 oligomers II: Sigma-2/PGRMC1 receptors mediate Abeta 42 oligomer binding and synaptotoxicity. PloS one 2014, 9 (11), e111899. [PubMed: 25390692]

55. Zheng X; Wu C; Liu D; Li H; Bitan G; Shea J-E; Bowers MT, Mechanism of C-Terminal Fragments of Amyloid β-Protein as Aβ Inhibitors: Do C-Terminal Interactions Play a Key Role in Their Inhibitory Activity? The Journal of Physical Chemistry B 2016, 120 (8), 1615–1623. [PubMed: 26439281]
56. de Almeida NEC; Do TD; LaPointe NE; Tro M; Feinstein SC; Shea JE; Bowers MT, 1,2,3,4,6-penta-O-galloyl-β-D-glucopyranose Binds to the N-terminal Metal Binding Region to Inhibit Amyloid β-protein Oligomer and Fibril Formation. Int J Mass Spectrom 2017, 420, 24–34. [PubMed: 29056865]
57. Mastrangelo IA; Ahmed M; Sato T; Liu W; Wang C; Hough P; Smith SO, High-resolution Atomic Force Microscopy of Soluble Aβ42 Oligomers. Journal of molecular biology 2006, 358 (1), 106–119. [PubMed: 16499926]
58. Kim JM; Jung HS; Park JW; Lee HY; Kawai T, AFM phase lag mapping for protein–DNA oligonucleotide complexes. Analytica Chimica Acta 2004, 525 (2), 151–157.
59. Round AN; Miles MJ, Exploring the consequences of attractive and repulsive interaction regimes in tapping mode atomic force microscopy of DNA. Nanotechnology 2004, 15 (4), S176.
60. García R; Magerle R; Perez R, Nanoscale compositional mapping with gentle forces. Nature Materials 2007, 6, 405. [PubMed: 17541439]
61. Gazit E, A possible role for π-stacking in the self-assembly of amyloid fibrils. The FASEB Journal 2002, 16 (1), 77–83. [PubMed: 11772939]
62. Marshall KE; Morris KL; Charlton D; O'Reilly N; Lewis L; Walden H; Serpell LC, Hydrophobic, Aromatic, and Electrostatic Interactions Play a Central Role in Amyloid Fibril Formation and Stability. Biochemistry 2011, 50 (12), 2061–2071. [PubMed: 21288003]
63. Bleiholder C; Do TD; Wu C; Economou NJ; Bernstein SS; Buratto SK; Shea J-E; Bowers MT, Ion Mobility Spectrometry Reveals the Mechanism of Amyloid Formation of Aβ(25–35) and Its Modulation by Inhibitors at the Molecular Level: Epigallocatechin Gallate and Scylloinositol. Journal of the American Chemical Society 2013, 135 (45), 16926–16937. [PubMed: 24131107]

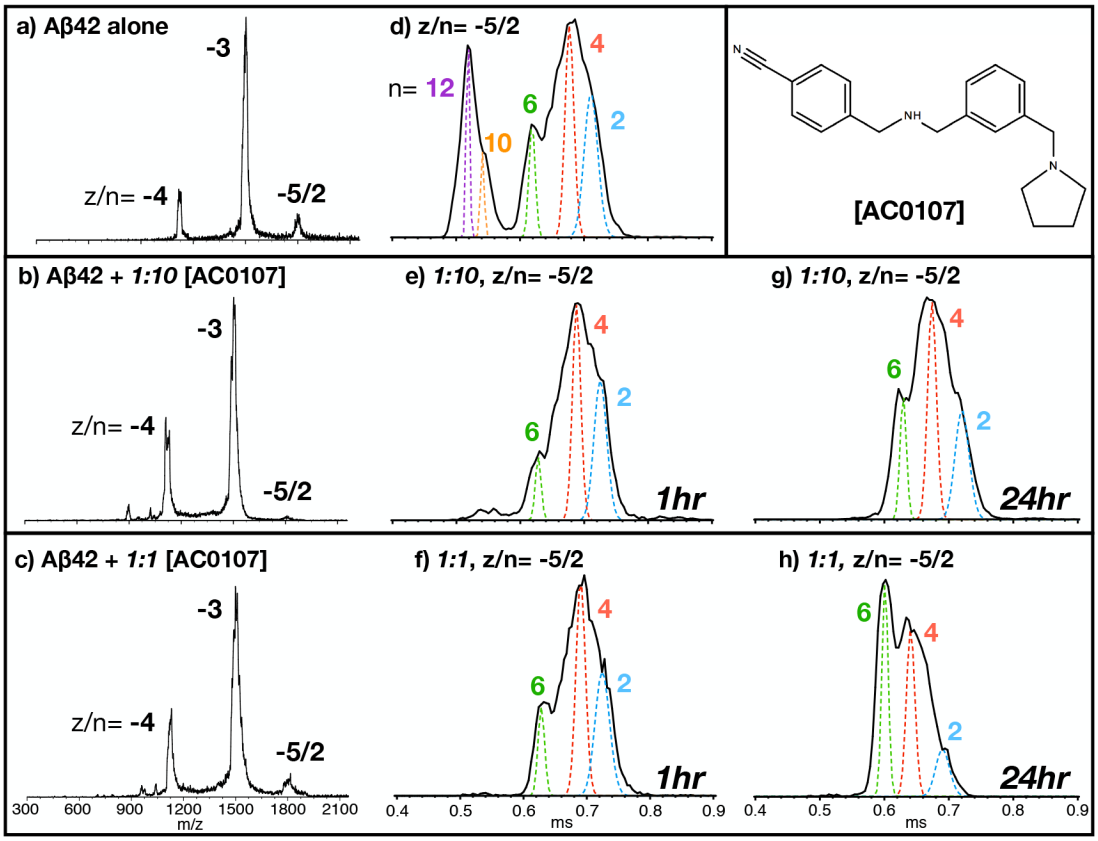

Figure 1.

a-c) Representative mass spectra for A03B242 alone, Aβ42 + 1:10 [AC0107], Aβ42 + 1:1 [AC0107], respectively. **d)** z/n= −5/2 ATD for Aβ42 alone. **e-f)** z/n= −5/2 ATDs at 1 hour co-incubation with 1:10 and 1:1 [AC0107], respectively. **g-h)** z/n= −5/2 ATD at 24 hours co-incubation with 1:10 and 1:1 [AC0107], respectively. The injection energy for each ATD is 40V. Each ATD has fitted structures with labels corresponding to Aβ42 dodecamer (n=12, purple fit), decamer (n=10, orange fit), hexamer (n=6, green fit), tetramer (n=4, red fit), and dimer (n=2, blue fit). The peak fitting procedure is outlined in the Supporting Information.

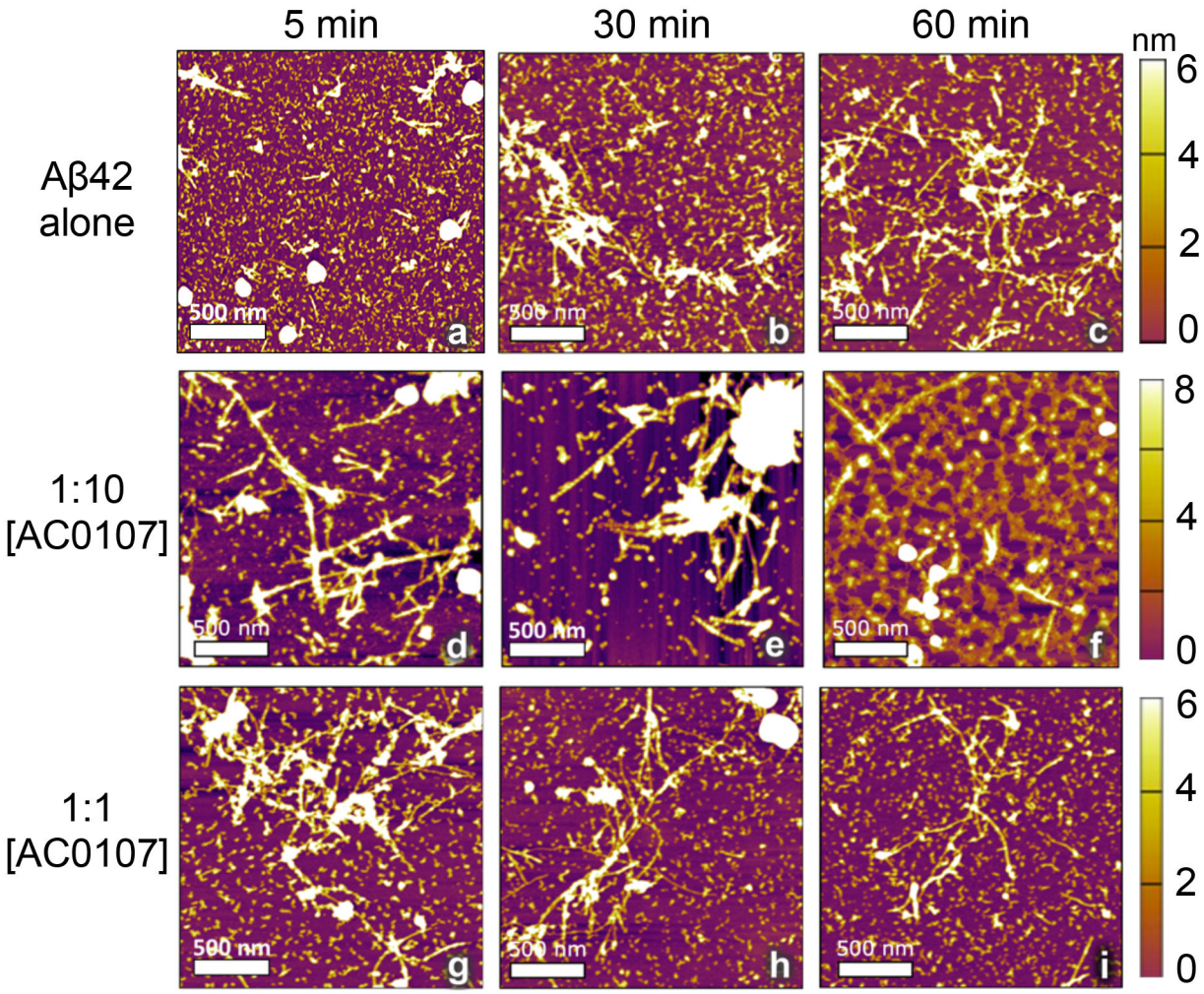

Figure 2.

AFM height images for representative 10 μM Aβ42 incubated alone at room temperature in solution for **a)** 5 min, **b)** 30 min, and **c)** 60 min. At 60 minutes, [AC0107] was added to the same solution of Aβ42 to a final concentration of 1:10 [AC0107] with aliquots taken and imaged at **d)** 5 min, **e)** 30 min, and **f)** 60 min co-incubation. **g)**, **h)**, **i)** are 5 min, 30 min, and 60 min co-incubation times, respectively, for 1:1 Aβ42:[AC0107] concentration after 60 minutes of Aβ42 incubated alone. Each image is 2 × 2 μm in dimension. Lighter colors are taller structures with the darkest representing the mica background surface. Particle height distributions are included in the Supporting Information.

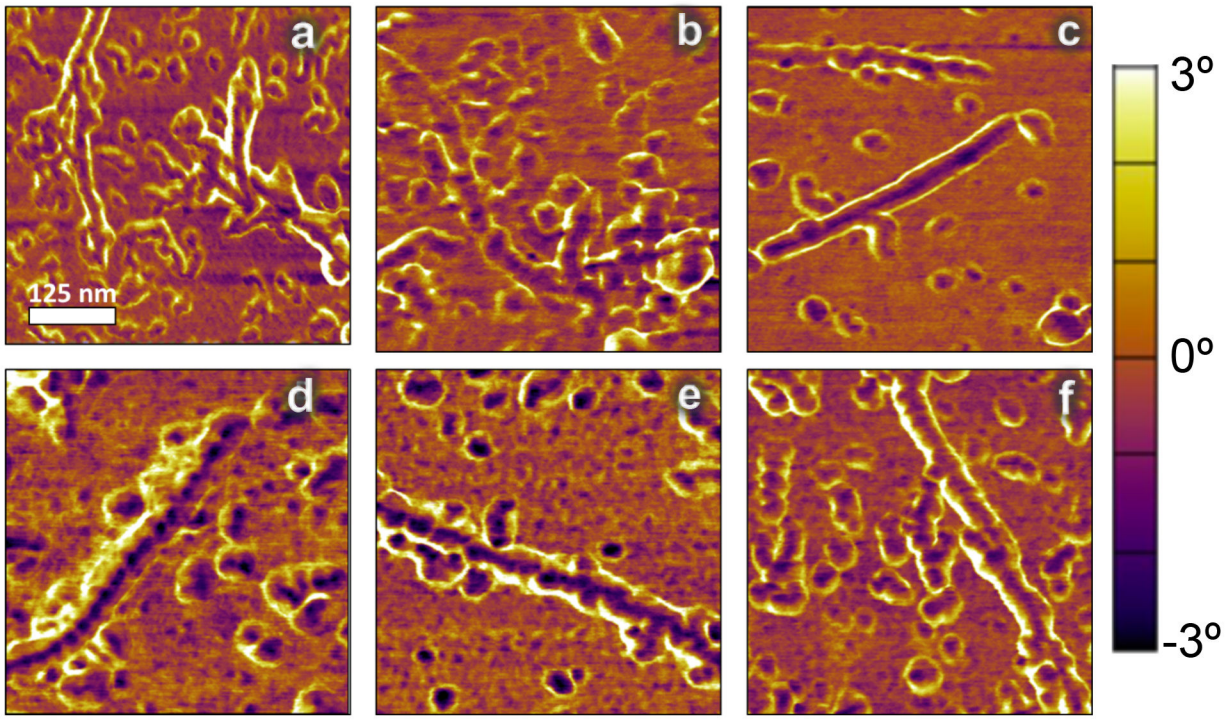

Figure 3.

AFM phase images of 10 μM Aβ42 alone at **a)** 5 min, **b)** 30 min, and **c)** 60 min incubation in solution. After 60 minutes, an equimolar 1:1 Aβ42:[AC0107] solution was achieved in the same solution and aliquots were removed and imaged at **d)** 5min, **e)** 30 min, and **f)** 60 min co-incubation. Relative to background media of the image, darker colors are physically harder and more structured than the surrounding material. Lighter colors are softer and less structured. Each image is 500nm × 500nm.

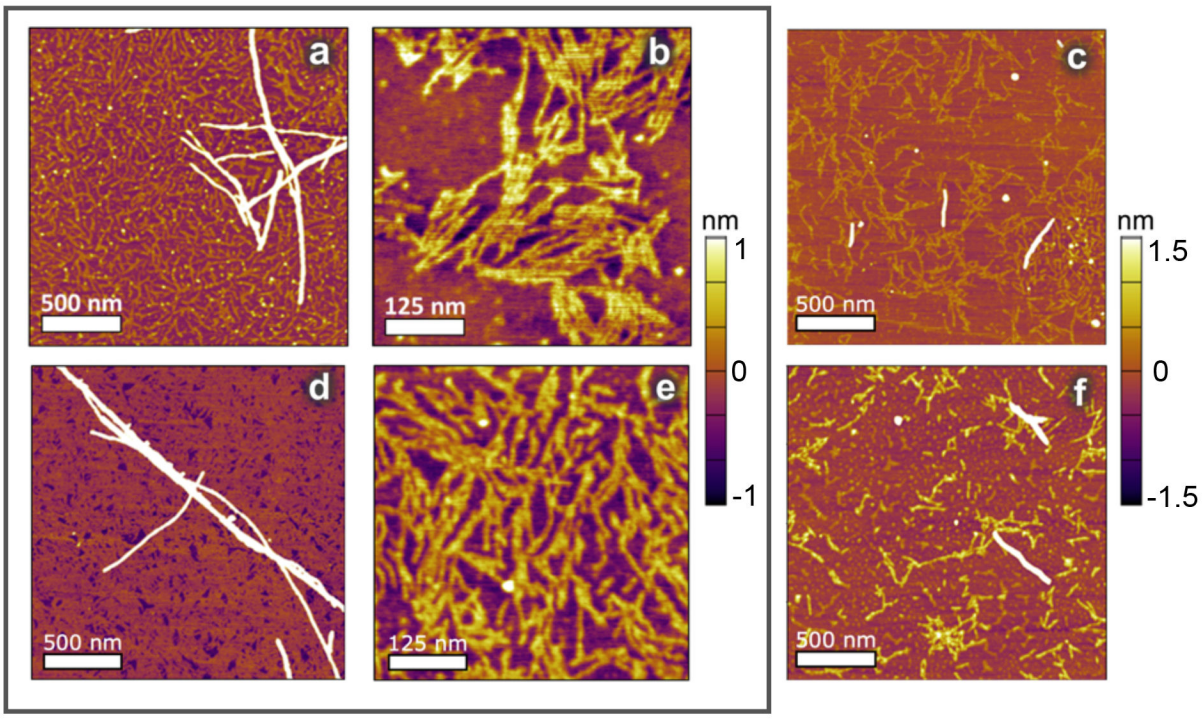

Figure 4.

AFM images at **a)** 24 hours co-incubation of 1:10 Aβ42:[AC0107] and at **c)** 48 hours. AFM images at **d)** 24 hours co-incubation of 1:1 Aβ42:[AC0107] and at **f)** 48 hours. **b)** and **e)** are zoomed in (500nm × 500nm) images of **a)** 1:10 and **d)** 1:1, respectively.

DAEFRHDSGY[10]EVHHQKLVFF[20]AEDVGSNKGA[30]IIGLMVGGVV[40]IA[42]

Scheme 1.
Peptide Sequence of Aβ42.

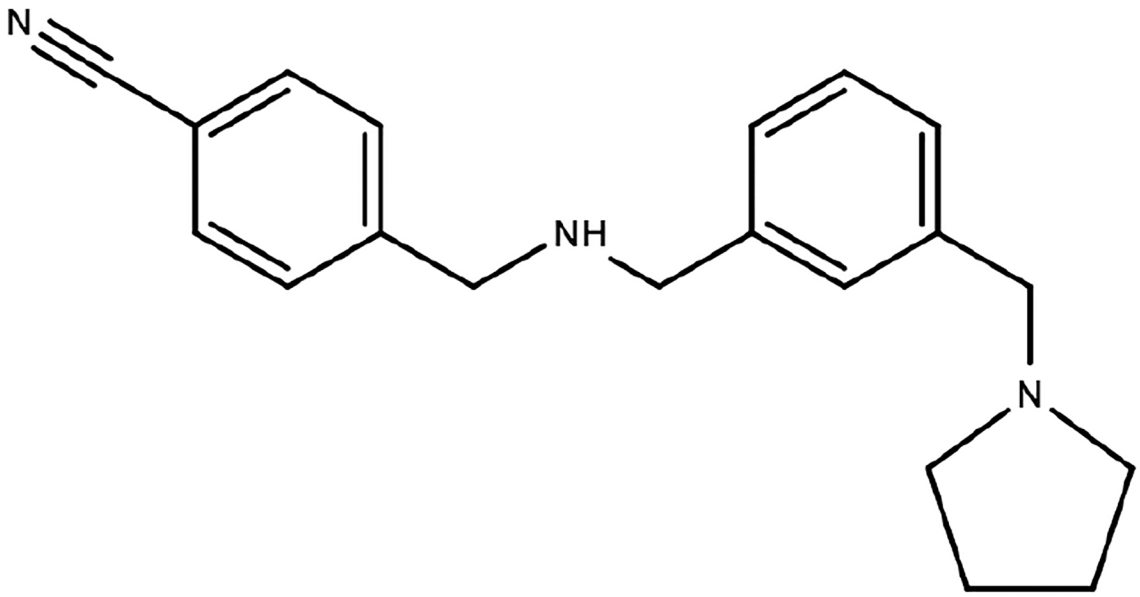

Scheme 2.
[AC0107]. 4-({[3-(1-Pyrrolidinylmethyl)benzyl]amino}methyl)benzonitrile

Table 1.

Collision Cross-Sections of Aβ42 before and after addition of [AC0107] in the z/n = −4, −3 and −5/2 ATDs.

			Collision Cross-Section (Å^2)*			
			1:10 [AC0107]		1:1 [AC0107]	
Oligomer	**Charge**	**Aβ42**	**1 hour**	**24 hours**	**1 hour**	**24 hours**
Monomer	−4	777	773	775	778	774
	−3	637	634	633	638	630
	−3	700	694	700	699	693
Dimer	−5	1278	1252	1260	1265	1253
Tetramer	−10	2357	2292	2251	2335	2196
Hexamer	−15	3023	2914	2991	2975	2921
Decamer	−20	3901	-	-	-	-
Dodecamer	−30	4312	-	-	-	-

*All cross sections are within 1.5% deviation